Langmuir

Pt Diffusion Dynamics for the Formation Cr−Pt Core−Shell Nanoparticles

G. Gupta,[†] P. Iqbal,[†] F. Yin,[‡,§] J. Liu,[‡] R. E. Palmer,[‡] S. Sharma,[†] K. Cham-Fai Leung,[∥] and P. M. Mendes*,[†]

[†]School of Chemical Engineering and [‡]Nanoscale Physics Research Laboratory, School of Physics and Astronomy, University of Birmingham, Edgbaston, Birmingham B15 2TT, U.K.

[§]School of Physics and Information Technology, Shaanxi Normal University, Xi'an 710062, China

[∥]Department of Chemistry and Institute of Creativity, Institute of Molecular Functional Materials, The Hong Kong Baptist University, University Grants Committee, Kowloon Tong, Kowloon, Hong Kong SAR

Ⓢ Supporting Information

ABSTRACT: Layered core−shell bimetallic Cr−Pt nanoparticles were prepared by the formation and later reduction of an intermediate Pt-ion-containing supramolecular complex onto preformed Cr nanoparticles. The resultant nanoparticles were characterized by X-ray diffraction analysis, transmission electron microscopy, X-ray photoelectron spectroscopy, and aberration-corrected scanning transmission electron microscopy. The results are consistent with the presence of Pt diffusion during or after bimetallic nanoparticle formation, which has resulted in a Pt/Cr-alloyed core and shell. We postulate that such Pt diffusion occurs by an electric-field-assisted process according to Cabrera−Mott theory and that it originates from the low work function of the preformed oxygen-defective Cr nanoparticles and the rather large electron affinity of Pt.
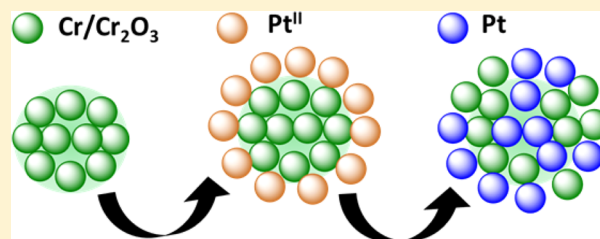
INTRODUCTION

Bimetallic nanoparticles are of wide interest due to the possibility to enhance or attain novel properties that cannot be reached in nanoparticles from pure metals.[1] Nanoparticles combining more than one metal in an alloy or core−shell configuration have been demonstrated to exhibit a spectrum of unique chemical, magnetic, and optical properties, leading to a wide range of potential applications, from catalysis and optoelectronics to magnetic storage and sensing.[2−8]

Core−shell nanoarchitectures are particularly attractive for property tuning through variations in several structural and chemical parameters such as core size, shell thickness, and chemical arrangement. It is in this context, for instance, that core−shell nanoparticles can be constructed in a manner in which the catalyst metal atoms are located in the shell layer, whereas the core can comprise a catalytically inactive, low-cost inorganic material. This architecture provides a potential way to significantly reduce the use of precious noble metals (e.g., Pt, Au, and Pd) and retain similar or superior catalytic activity compared to that of the pure metal nanocatalyst.[9,10] A salient target of such investigations is the incorporation of non-noble transition metals, such as Cu, Co, Ni, Fe, and Cr, within the core, which is surrounded by a Pt shell layer.[11−16] Although the synthesis and characterization of such core−shell nano-architectures have motivated numerous experimental and theoretical studies, it should be recognized that non-noble transition metals often exhibit the undesirable propensity to oxidize.[17,18]

During wet-chemical synthesis of core−shell structures, the non-noble metals usually get oxidized due to the presence of a reactive environment, resulting in oxide formation in the metal core. For instance, Ravel et al.[19] reported the formation of an Fe−Au core−shell prepared by a microemulsion technique in which the Fe component was found to be extensively oxidized. In another example, a Cu core with porous Mn_3O_4 shell nanoparticles was synthesized by the successive reduction of metal salts.[20] Despite using inert atmospheric conditions, the nanoparticles contained Cu oxide as revealed by X-ray absorption near-edge structure.

When transition metals undergo oxidation, it is important to consider their abilities to assume multiple oxidation states and thus different electron configurations. As a matter of fact, it is this particular feature of transition-metal oxides that make them highly susceptible to different types of structural defects.[17,21] These defects, which include point defects such as vacancies and interstitials, can differ from the bulk to the surface.[21] A striking and direct consequence of such defects is that metal and oxygen diffusion may occur through the oxide layer, as previously observed on macroscopic metal oxide structures.[22,23]
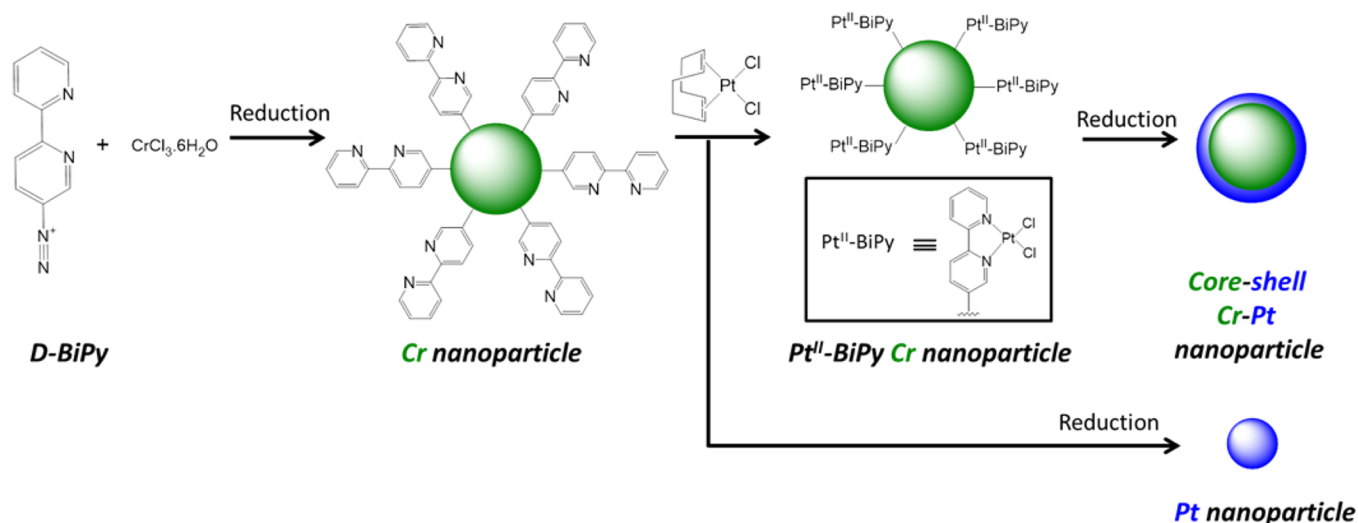
Figure 1. Proposed stepwise reaction sequence for the preparation of layered core−shell bimetallic Cr−Pt nanoparticles in one pot. Note that Pt[II]−Bipy represents not only individual Pt(II) metal ions being assembled with BiPy but also minuscule clusters consisting of very few Pt(II) ions and Pt(0) atoms.
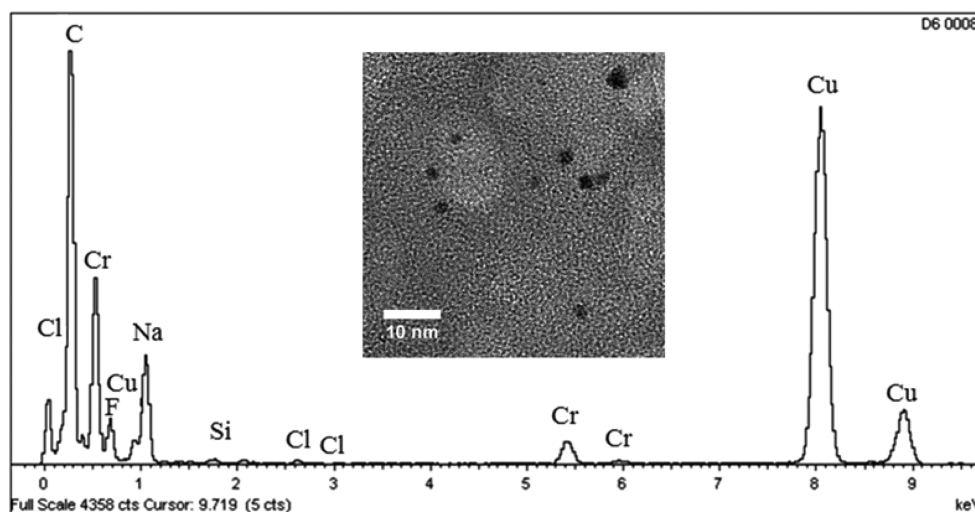

Figure 2. EDX spectrum of Cr nanoparticles. (Inset) TEM image of Cr nanoparticles.

Ocal et al.[22] have reported the diffusion of Au atoms through an O-deficient aluminum oxide layer to the oxide−metal interface. In contrast, a nondefective aluminum oxide film of similar thickness prevented any Au diffusion. These results have been interpreted on the basis of Cabrera−Mott theory,[24] in which diffusion is facilitated by the electric field created by the Mott potential. In this context, defective films suffer from low work functions, making them more prone to diffusion by high electron affinity metals such as Au. These observations pose the question of whether metal diffusion behavior through transition-metal oxides can be present and occur in a similar fashion in the reduced dimensionality of nanoparticles. To our knowledge, there are neither theoretical nor experimental data that support or rule out such a diffusion phenomenon. In order to provide new insights and understanding on the subject, herein we report on the wet-chemical synthesis and characterization of layered core−shell nanoparticles comprising the transition metal Cr as the core and the high electron affinity Pt as the shell. Crucial to this investigation was a thorough characterization and analysis of the formed nanoparticles using several techniques, including transmission electron microscopy

(TEM) with energy dispersive X-ray spectroscopy (EDX), X-ray diffraction (XRD), X-ray photoelectron spectroscopy (XPS), and aberration-corrected scanning transmission electron microscopy (STEM).

■ RESULTS AND DISCUSSION

The synthesis strategy for the preparation of core−shell Cr−Pt nanoparticles is illustrated in Figure 1.

This strategy aims at generating nanoparticles with a Pt shell on a Cr core and involves four steps: (1) the synthesis of a bipyridine Pt-chelating moiety[25−27] containing a diazonium cation (D-BiPy) (see Supporting Information for details on the D-BiPy synthesis and characterization); (2) the formation of **D-BiPy**-functionalized Cr core nanoparticles stabilized by Cr−C bonds via diazonium reduction; (3) the complexation of Pt(II) metal ions with the bipyridine chelating moieties of the **D-BiPy**-functionalized Cr core nanoparticles; and (4) the reduction of the Pt(II) metal ions on the preformed Cr nanoparticles to their zero-valent state. In our one-pot synthesis where the reducing agent is present throughout but with

diminished reducing power in the complexation stage, there are two possible routes for complexation leading to the deposition of Pt on the preformed nanoparticles. One route is the complexation of **BiPy** with Pt(II) metal ions and the other is the complexation of **BiPy** with minuscule clusters consisting of very few Pt(II) metal ions and Pt(0) atoms.[4,5] The Pt precursor that is not involved in complex formation with the bipyridine chelating moieties can form pure Pt nanoparticles.

TEM with EDX was used to determine the particle size, the dispersion, and the elemental composition of Cr nanoparticles. The EDX spectrum (Figure 2) confirms the formation of Cr nanoparticles and the presence of a significant amount of oxygen. Because the preparation of the Cr nanoparticles was conducted under ambient conditions and given chromium's propensity to oxidize,[17] it can be inferred that the presence of oxygen on the Cr nanoparticles originates from the formation of Cr oxide. The inset of Figure 2 shows a TEM image of the **D-BiPy**-functionalized Cr core nanoparticles, which are well dispersed and have an average size of 1.8 ± 0.3 nm.

XRD, XPS, and STEM analyses were performed to fully characterize the synthesized Cr−Pt nanoparticles. The XRD pattern of the synthesized Cr−Pt nanoparticles is shown in Figure S2. The peaks corresponding to the face-centered-cubic (FCC) structure of Pt are all present in the spectrum and labeled accordingly. The extra peaks around 32 and 58° arise from the substrate material. The crystallite size of Cr−Pt nanoparticles is calculated using the Scherer equation[28] and is found to be 2.3 nm. The lattice parameter for Cr−Pt is also calculated to be 3.91 Å, which is close to the lattice parameter for Pt (3.92 Å).[29] Note that we have also investigated over 180 nanoparticles by STEM and found that ∼45% of the nanoparticles have face-centered-cubic (FCC) structures, ∼5% have icosahedral structures, and the rest of the nanoparticles are amorphous or unclassified. The XRD results suggest that Pt is present in high amounts in the synthesized nanoparticles. This finding indicates that the Pt precursor, which was not involved in complex formation with the bipyridine chelating moieties, had undergone reduction and the formation of pure Pt nanoparticles.

Survey and high-resolution XPS spectra of N 1s, O 1s, Cr 2p, and Pt 4f were acquired for the Cr−Pt nanoparticles. Several samples were analyzed, and the results presented herein are based on a sample area where both Cr and Pt are present. It is important to note, however, that XPS analysis of some sample areas indicated only the presence of Pt and not Cr. This observation is in agreement with the XRD data and confirmed that pure Pt nanoparticles were also formed during the preparation of the layered core−shell Cr−Pt nanoparticles.

The XPS N 1s spectrum (Figure 3a) can be assigned to a single peak centered at 399.7 eV, which can be ascribed to the pyridine nitrogen in the D-BiPy molecule. The O 1s spectrum (Figure 3b) contains a single peak centered at 531.4 eV, which suggests the presence of metal (either Cr or Pt) oxide and/or hydroxide on the Cr−Pt nanoparticles. The Cr 2p spectrum (Figure 3c) can be resolved into two doublets, indicating that Cr exists in metallic as well as oxidized form. The doublet with peaks located at 577.5 and 587.3 eV is assigned to chromium oxide in its oxidized state (III).[30,31] Among the different chromium oxides, Cr_2O_3 is the most stable[32] and thus is expected to be the main form of chromium oxide in the synthesized Cr−Pt nanoparticles. The other doublet with binding energy values of 576.4 and 585.6 eV is attributed to metallic Cr.[30] The ratio of oxidized Cr to metallic Cr, as
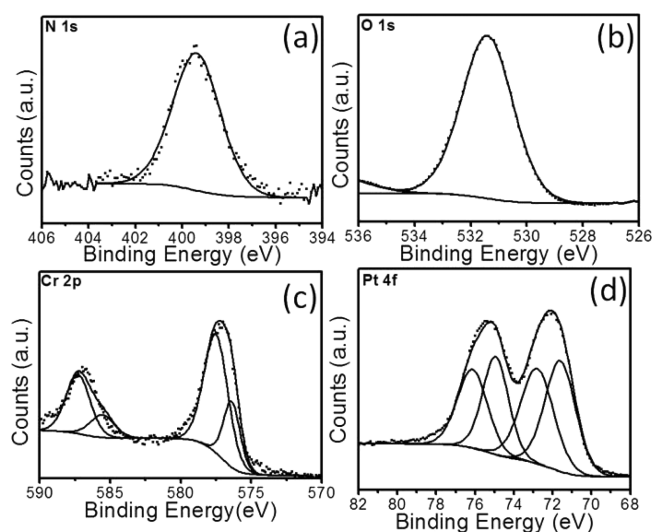
Figure 3. XPS spectra of the N 1s, O 1s, Cr 2p, and Pt 4f peak regions of the synthesized Cr−Pt nanoparticles.

calculated by the integrated intensities of the two doublet peaks, is 4:1. The analysis of the Pt spectrum suggests the presence of metallic Pt with a doublet at 71.6 and 74.9 eV and a similar amount of $Pt(OH)_2$ (doublet at 72.8 and 76.1 eV).[30]

From the XRD and XPS analysis, the formation of core−shell Cr−Pt cannot be established. However, this analysis reveals the presence of Pt and Cr in the nanoparticles and that a high percentage of Cr exists in its oxidized form. In order to gain insight into the atomic structure of the Pt−Cr nanoparticles, STEM studies were performed. Because STEM uses Z (atomic number) contrast imaging, the intensity in the HAADF images is quite sensitive to the atomic number of the materials.[33−35] The HAADF intensity (I) is proportional to Z^n, where $n = 1.46 ± 0.18$ for our STEM.[36] Because the atomic number of Pt is 78 and that of Cr is 24, the HAADF intensity of one Pt atom is about 5.59 times brighter than that of one Cr atom. Hence, chemical contrast can be obtained by the analysis of the HAADF contrast within bimetallic nanoparticles.

Figure 4 shows representative aberration-corrected STEM images and diameter distributions of Cr−Pt nanoparticles. Two kinds of nanoparticles (small and large) can be seen in the STEM image. The corresponding distribution of diameters is shown in Figure 4b. The statistical data show that the diameter of the smaller nanoparticles is 1.45 ± 0.25 nm and that the diameter of the larger nanoparticles is 2.35 ± 0.30 nm. The size of the smaller nanoparticles is lower when compared to that of D-BiPy-functionalized Cr core nanoparticles (∼1.8 nm as determined by TEM). This finding suggests that the smaller nanoparticles are neither pure Cr nor bimetallic nanoparticles but pure Pt nanoparticles. This conclusion is supported by the XRD and XPS data.

Additionally, from the relationship of HAADF intensity versus the volume of the particles (Figure 5), we can observe that most of the data points are under the fitting line when $R^3 > 2$, indicating a lower percentage of Pt (Pt %) in larger clusters. This trend in intensity can be seen clearly in Figure 5b, which shows the diagram of the average value of HAADF intensity against the cluster volume (R^3). These results reveal that the smaller nanoparticles ($R^3 < 2$) have the highest average HAADF intensity, enabling us to ascribe them as pure Pt nanoparticles.
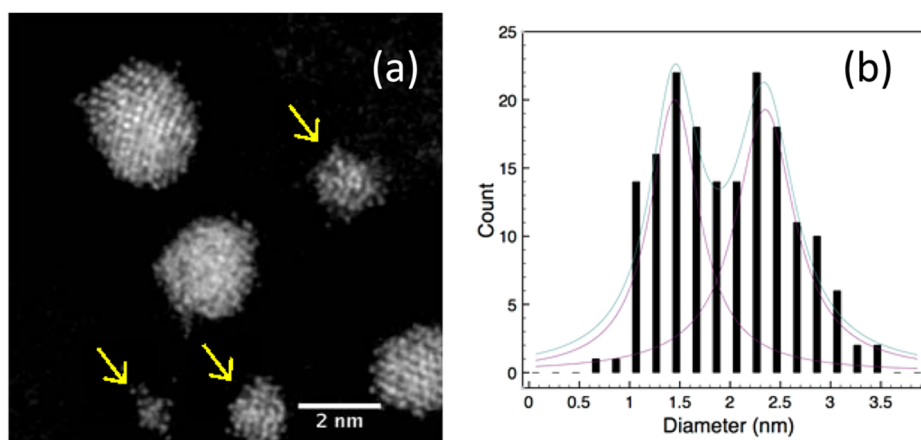
Figure 4. STEM image and diameter distribution of Cr−Pt nanoparticles: (a) STEM image and (b) diameter distribution. The positions of the two peaks are at 1.45 ± 0.25 and 2.35 ± 0.30 nm, respectively. Small particles are indicated with arrows.
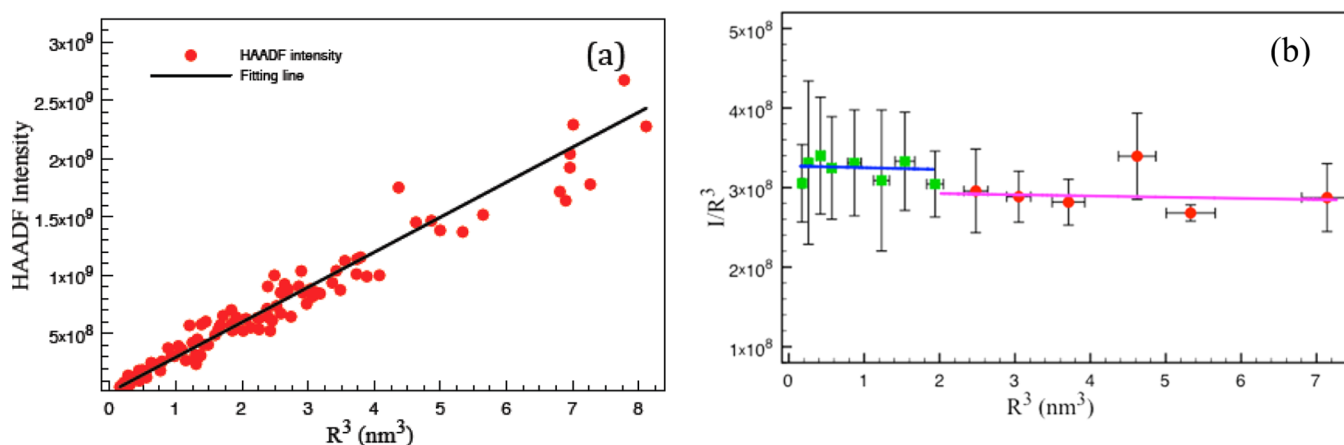

Figure 5. Relationship between the HAADF intensity and cluster volume (a) and (b) average HAADF intensity against the cluster volume.
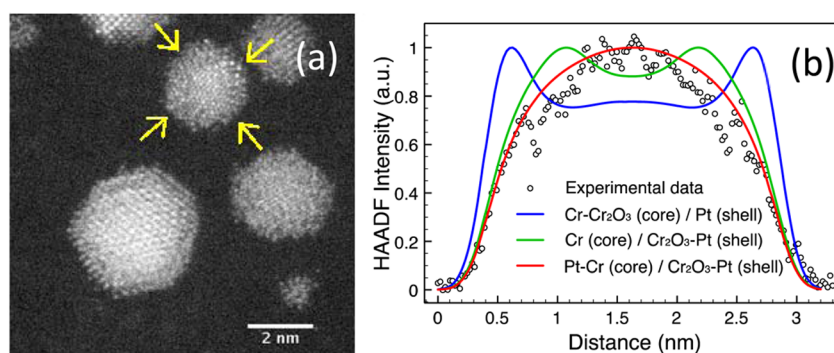

Figure 6. (a) High-resolution STEM image and (b) experimental and simulated HAADF intensity line profiles for Cr−Pt nanoparticles. Hollow circles: the experimental average profile was measured along the two lines pointed to by arrows with 4.1-Å-wide bands. The red curve denotes the intensity profile calculated from the model of a Pt−Cr core and a Cr_2O_3−Pt shell. Green indicates the model of a Cr core and Cr_2O_3/Pt shell. Blue indicates the model of a Cr−Cr_2O_3 core and Pt shell.

On the other hand, the larger nanoparticles, which exhibit a diameter 0.55 nm larger than the diameter of the D-BiPy-functionalized Cr core nanoparticles, are expected to be the Cr−Pt nanoparticles. Thus, further STEM analysis is focused on these particles. Figure 6a displays typical, high-resolution, aberration-corrected STEM images of the Cr−Pt nanoparticles. From the image, we can see that the Cr−Pt nanoparticles do not display a typical Cr core/Pt shell structure (dark core and bright shell). It can be seen very clearly in the profile in Figure

6b. The HAADF intensity profile of the Cr−Pt nanoparticles reveals that the central areas of the nanoparticles are either similar to or brighter than the edge areas and exhibit a nearly flat contrast at the core. It indicates that no Pt shell was formed on the Cr−Pt nanoparticles.

In order to identify the structure of the Cr−Pt nanoparticles, we simulated the STEM intensity profiles of model core−shell morphologies. Simple geometrical structures were employed: both the core and the shell are spherical, and the center of mass

of the core is the same as the center of mass of the shell. The HAADF intensities depend exclusively on the height of the projected atomic column, with each atom contributing a $Z^{1.46}$-dependent intensity.[32] On the basis of the TEM and STEM results, we employed Cr−Pt nanoparticles of diameter 2.35 nm with a 1.8 nm core. Furthermore, we assume that the core is Cr−Cr_2O_3 and the ratio of oxidized Cr is 80%, as determined by XPS analysis. The calculated HAADF intensity profiles were convolved with a Gaussian function.

The simulated HAADF intensity profiles of three kind of structures of Cr−Cr_2O_3 (core)/Pt (shell), Cr (core)/ Cr_2O_3−Pt (shell) and Pt−Cr (core)/Cr_2O_3−Pt (shell) are displayed in Figure 7. Compared to the experimental profile, we can see that
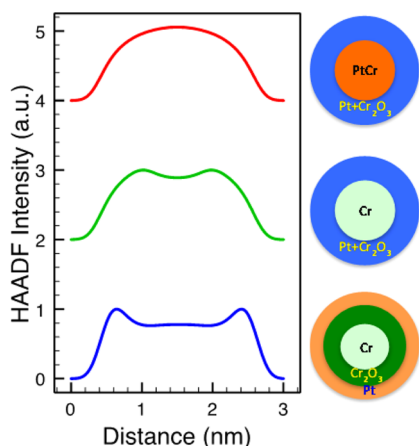

Figure 7. Simulated HAADF intensity line profiles for three types of bimetallic Cr−Pt nanoparticles and their corresponding models on the right.

the experimental HAADF intensity profile (hollow circles in Figure 6b) is not consistent with the HAADF intensity profiles calculated from the structure of Cr−Cr_2O_3 (core)/Pt(shell) or Cr (core)/Cr_2O_3−Pt (shell). The HAADF intensity profile of the Pt−Cr (core)/Cr_2O_3−Pt (shell) structure agrees well with the experimental profiles. The statistical analysis of 182 Cr−Pt nanoparticles has revealed that 98% of the particles exhibit a profile similar to that mentioned above (i.e., Pt−Cr (core)/ Cr_2O_3−Pt (shell)). Only 2% of the particles exhibited concave HAADF intensity line profiles (i.e., Pt-rich shell) as depicted in Figure S3.

These findings mean that the Pt atoms have diffused from the surface into the core and formed a Pt−Cr alloy core and Cr_2O_3−Pt shell. The diffusion of Pt atoms can be explained by Cabrera−Mott theory. On the basis of the theory, the Mott potential will be built up across the oxide layer due to a contact potential difference between metal and adsorbed oxygen.[20] This potential drives both anion and cation transport across the oxide film at low temperature, where the anions will diffuse into the metal core. Because of the high electron affinity of Pt, when the Pt atom deposits on the oxide layer, it will tend to diffuse into the core of the bimetallic nanoparticles through the well-established field-assisted diffusion mechanism.[18] This behavior leads to the formation of the observed Pt−Cr (core)/Cr_2O_3− Pt (shell) nanoparticles.

CONCLUSIONS

We have synthesized layered core−shell bimetallic Cr−Pt nanoparticles by the formation and later reduction of an intermediate Pt-ion-containing supramolecular complex onto preformed Cr nanoparticles. By performing TEM, XRD, XPS, and STEM analysis, we studied in detail the composition and structure of the synthesized Cr−Pt nanoparticles. The results are consistent with the occurrence of Pt diffusion during or after bimetallic nanoparticle formation, which results in a Pt/ Cr-alloyed core and shell. This behavior is tentatively attributed to field-assisted diffusion by a Mott−Cabrera-type mechanism. This study highlights a crucial but often overlooked diffusion phenomenon that must be considered if core−shell nanoparticles are developed on the basis of non-noble transition metals.

EXPERIMENTAL SECTION

Synthesis of Layered Cr−Pt Core−Shell Nanoparticles. The D-BiPy compound used in the synthesis of the Cr−Pt core−shell nanoparticles was freshly prepared and characterized as detailed in the Supporting Information and immediately used. Briefly, D-BiPy was dissolved in ethanol (10 mL, 6 mM) and mixed with a solution of $CrCl_3 \cdot 6H_2O$ in ethanol (5 mL, 6 mM) under continuous stirring in a round-bottomed flask at 500 rpm using a magnetic stirrer for 10 min. A freshly prepared $NaBH_4$ solution in ethanol (5 mL, 0.4 M) was slowly added to the mixture, and a change in color to dark green was observed, suggesting the reduction of the Cr precursor. After 30 min, a solution of dichloro(1,5-cyclooctadiene)platinum(II) in ethanol (5 mL, 6 mM) was slowly added to the mixture. A change in color of the mixture was observed after 20−30 s, suggesting the reduction of the Pt precursor. The nanoparticles were purified by precipitation from ethanol using acetone, followed by centrifugation, and the supernatant was discarded. The precipitation/centrifugation was repeated three more times, after which the black solid was dried in a vacuum oven at 40 °C.

Transmission Electron Microscopy (TEM). The nanoparticles were deposited on Cu grids with a carbon coating on one side and examined in an FEI Tecnai TF20 coupled with an Oxford Instruments INCA 350 EDX system operated at an acceleration voltage of 200 kV. Bright-field images were taken at low and high resolution to analyze the size, size distribution, and structure of the nanoparticles. EDX was done on the individual particles as well as over different areas to study the composition of the particles. The particle size was calculated by analyzing the high-resolution images using ImageJ.

X-ray Diffraction (XRD). Laboratory-source XRD (INEL XRD Equinox 3000 diffractometer) was used to characterize the structure of the nanoparticles. The Cu Kα source operates at a potential of 40 kV and a current of 40 mA. This diffractometer can measure the whole 2θ range simultaneously, i.e., 0−120°. An aluminum XRD sample holder of size 3 cm × 3 cm is used. The holder has a well in the center of size 1 cm width × 1 cm length × 1 mm depth to hold the powder samples. The Cr−Pt nanoparticle powder was poured into the well and carefully flattened to form a smooth surface in alignment with the surface of the aluminum. The diffraction pattern was analyzed using Match software. Instrumental broadening was determined using Si standard samples, and the particle size was estimated using the observed line broadening and Scherer equation at different planes of reflection.

X-ray Photoelectron Spectroscopy (XPS). XPS spectra were obtained on the AXIS Nova (Kratos Analytical) instrument based at the University of Newcastle (NEXUS), U.K. XPS experiments were carried out using a monochromatic Al Kα X-ray source (1486.7 eV) and a takeoff angle of 90° with respect to the surface plane. High-resolution scans of Pt 4f, C 1s, O 1s, and Cr 2p were recorded using a pass energy of 20 eV with a step size of 0.1 eV. Fitting of XPS peaks was performed using CASA XPS processing software. Sensitivity factors used in this study were C 1s, 1.00; O 1s, 2.8; Pt $4f_{7/2}$, 8.65; Pt $4f_{5/2}$, 6.8; Cr $2p_{3/2}$, 7.69; and Cr $2p_{1/2}$, 3.98.

Scanning Transmission Electron Microscope (STEM). The STEM investigation was performed in a 200 kV JEOL 2100F instrument equipped with a CEOS spherical aberration probe

corrector. The inner and outer collection angles of the HAADF detector were set to 62 and 164 mrad, respectively, and the probe convergence angle was 19 mrad. The images were taken in 3 s with an electron dose of ~4.6 × 10^4 electrons/Å^2. The particle size and intensity profiles were obtained by analyzing the HAADF images using ImageJ (http://imagej.nih.gov/ij/).

■ ASSOCIATED CONTENT

ⓢ Supporting Information

D-BiPy synthesis and characterization in addition to HAADF intensity analysis. The Supporting Information is available free of charge on the ACS Publications website at DOI: 10.1021/acs.langmuir.5b01410.

■ AUTHOR INFORMATION

Corresponding Author
*E-mail: p.m.mendes@bham.ac.uk.

Notes
The authors declare no competing financial interest.

■ ACKNOWLEDGMENTS

■ REFERENCES

(1) Ghosh Chaudhuri, R.; Paria, S. Core/Shell Nanoparticles: Classes, Properties, Synthesis Mechanisms, Characterization, and Applications. *Chem. Rev.* **2012**, *112*, 2373−2433.

(2) Bing, Y.; Liu, H.; Zhang, L.; Ghosh, D.; Zhang, J. Nanostructured Pt-Alloy Electrocatalysts for PEM Fuel Cell Oxygen Reduction Reaction. *Chem. Soc. Rev.* **2010**, *39*, 2184−2202.

(3) Hu, J. G.; He, B.; Lu, J.; Hong, L. J.; Yuan, J. H.; Song, J. X.; Niu, L. Facile Preparation of Pt/Polyallylamine/Reduced Graphene Oxide Composites and Their Application in the Electrochemical Catalysis on Methanol Oxidation. *Int. J. Electrochem. Sci.* **2012**, *7*, 10094−10107.

(4) West, J. L.; Halas, N. J. Engineered Nanomaterials for Biophotonics Applications: Improving Sensing, Imaging, and Therapeutics. *Annu. Rev. Biomed. Eng.* **2003**, *5*, 285−292.

(5) Frey, N. A.; Peng, S.; Cheng, K.; Sun, S. Magnetic Nanoparticles: Synthesis, Functionalization, and Applications in Bioimaging and Magnetic Energy Storage. *Chem. Soc. Rev.* **2009**, *38*, 2532−2542.

(6) Li, C.; Yamauchi, Y. Facile solution synthesis of Ag@Pt core-shell nanoparticles with dendritic Pt shells. *Phys. Chem. Chem. Phys.* **2013**, *15*, 3490−3496.

(7) Ataee-Esfahani, H.; Imura, M.; Yamauchi, Y. All-metal mesoporous nanocolloids: solution-phase synthesis of core-shell Pd@Pt nanoparticles with a designed concave surface. *Angew. Chem.* **2013**, *52*, 13611−13615.

(8) Wang, L.; Yamauchi, Y. Autoprogrammed synthesis of triple-layered Au@Pd@Pt core-shell nanoparticles consisting of a Au@Pd bimetallic core and nanoporous Pt shell. *J. Am. Chem. Soc.* **2010**, *132*, 13636−13638.

(9) Adams, B. D.; Ostrom, C. K.; Chen, A. Highly Active PdPt Catalysts for the Electrochemical Reduction of H$_2$O$_2$. *J. Electrochem. Soc.* **2011**, *158*, B434.

(10) Kundu, S.; Nagaiah, T. C.; Xia, W.; Wang, Y. M.; Van Dommele, S.; Bitter, J. H.; Santa, M.; Grundmeier, G.; Bron, M.; Schuhmann, W.; Muhler, M. Electrocatalytic Activity and Stability of Nitrogen-Containing Carbon Nanotubes in the Oxygen Reduction Reaction. *J. Phys. Chem. C* **2009**, *113*, 14302−14310.

(11) Bezerra, C.; Zhang, L.; Lee, K.; Liu, H.; Marques, A.; Marques, E.; Wang, H.; Zhang, J. A Review of Fe−N/C and Co−N/C Catalysts for the Oxygen Reduction Reaction. *Electrochim. Acta* **2008**, *53*, 4937−4951.

(12) Jeon, M. K.; Zhang, Y.; McGinn, P. J. Effect of Reduction Conditions on Electrocatalytic Activity of a Ternary PtNiCr/C Catalyst for Methanol Electro-oxidation. *Electrochim. Acta* **2009**, *54*, 2837−2842.

(13) Chen, Y. M.; Yang, F.; Dai, Y.; Wang, W. Q.; Chen, S. L. Ni@Pt Core-Shell Nanoparticles: Synthesis, Structural and Electrochemical Properties. *J. Phys. Chem. C* **2008**, *112*, 1645−1649.

(14) Long, N. V.; Yang, Y.; Minh Thi, C.; Minh, N. V.; Cao, Y.; Nogami, M. The Development of Mixture, Alloy, and Core-Shell Nanocatalysts with Nanomaterial Supports for Energy Conversion in Low-Temperature Fuel Cells. *Nano Energy* **2013**, *2*, 636−676.

(15) Sarkar, A.; Manthiram, A. Synthesis of Pt@Cu Core-Shell Nanoparticles by Galvanic Displacement of Cu by Pt^{4+} Ions and Their Application as Electrocatalysts for Oxygen Reduction Reaction in Fuel Cells. *J. Phys. Chem. C* **2010**, *114*, 4725−4732.

(16) Ghosh, D.; Chen, S. Palladium Nanoparticles Passivated by Metal-Carbon Covalent Linkages. *J. Mater. Chem.* **2008**, *18*, 755−762.

(17) Korotcenkov, G. Metal Oxides for Solid-State Gas Sensors: What Determines our Choice? *Mater. Sci. Eng., B* **2007**, *139*, 1−23.

(18) Barnhart, J. Occurrences, Uses, and Properties of Chromium. *Regul. Toxicol. Pharmacol.* **1997**, *26*, S3−S7.

(19) Ravel, B.; Carpenter, E. E.; Harris, V. G. Oxidation of Iron in Iron/Gold Core/Shell Nanoparticles. *J. Appl. Phys.* **2002**, *91*, 8195.

(20) Subramanian, N. D.; Moreno, J.; Spivey, J. J.; Kumar, C. Copper Core-Porous Manganese Oxide Shell Nanoparticles. *J. Phys. Chem. C* **2011**, *115*, 14500−14506.

(21) Ganduglia-Pirovano, M. V.; Hofmann, A.; Sauer, J. Oxygen Vacancies in Transition Metal and Rare Earth Oxides: Current State of Understanding and Remaining Challenges. *Surf. Sci. Rep.* **2007**, *62*, 219−270.

(22) Ocal, C.; Ferrer, S.; García, N. Cabrera-Mott Mechanism for Oxidation of Metals Explains Diffusion of Metallic Atoms Through Thin Defective Oxide Layers. *Surf. Sci.* **1985**, *163*, 335−356.

(23) Ocal, C.; Ferrer, S. Low Temperature Diffusion of Pt and Au Atoms Through Thin TiO$_2$ Films on a Ti Substrate. *Surf. Sci.* **1987**, *191*, 147−156.

(24) Cabrera, N.; Mott, N. F. Theory of the Oxidation of Metals. *Rep. Prog. Phys.* **1948**, *12*, 163−184.

(25) Weinstein, J. A.; Zheligovskaya, N. N.; Mel'nikov, M. Y.; Hartl, F. Spectroscopic (UV/VIS, resonance Raman) and spectroelectrochemical study of platinum(II) complexes with 2,2 '-bipyridine and aromatic thiolate ligands. *J. Chem. Soc., Dalton Trans.* **1998**, 2459−2466.

(26) Tang, W. S.; Lu, X. X.; Wong, K. M. C.; Yam, V. W. W. Synthesis, photophysics and binding studies of Pt(II) alkynyl terpyridine complexes with crown ether pendant. Potential luminescent sensors for metal ions. *J. Mater. Chem.* **2005**, *15*, 2714−2720.

(27) Muro, M. L.; Diring, S.; Wang, X. H.; Ziessel, R.; Castellano, F. N. Photophysics in Platinum(II) Bipyridylacetylides. *Inorg. Chem.* **2009**, *48*, 11533−11542.

(28) Cullity, B. D.; Stock, S. R.: *Elements of X-ray Diffraction*, 3rd ed.; Prentice-Hall, 2001.

(29) Hermann, K.: *Crystallography and Surface Structure: An Introduction for Surface Scientists and Nanoscientists*; Wiley-VCH Verlag GmbH & Co. KGaA, 2011.

(30) Moulder, J. F.; Stickle, W. F.; Sobol, P. E.; Bomben, K. D.: *Handbook of X-ray Photoelectron Spectroscopy*; Physical Electronics: Minnesota, 1995.

(31) Biesinger, M. C.; Brown, C.; Mycroft, J. R.; Davidson, R. D.; McIntyre, N. S. X-Ray Photoelectron Spectroscopy Studies of Chromium Compounds. *Surf. Interface Anal.* **2004**, *36*, 1550−1563.

(32) Brady, P. V. *The Physics and Chemistry of Mineral Surfaces*; CRC Press, 1996.

(33) Li, Z. Y.; Wilcoxon, J. P.; Yin, F.; Chen, Y.; Palmer, R. E.; Johnston, R. L. Structures and Optical Properties of 4−5 nm Bimetallic AgAu Nanoparticles. *Faraday Discuss.* **2008**, *138*, 363.

(34) Yin, F.; Wang, Z. W.; Palmer, R. E. Controlled Formation of Mass-Selected Cu-Au Core-Shell Cluster Beams. *J. Am. Chem. Soc.* **2011**, *133*, 10325−10327.

(35) Yin, F.; Wang, Z. W.; Palmer, R. E. Ageing of Mass-Selected Cu/Au and Au/Cu Core/Shell Clusters Probed with Atomic Resolution. *J. Exp. Nanosci.* **2012**, *7*, 703−710.

(36) Wang, Z. W.; Palmer, R. E. Intensity Calibration and Atomic Imaging of Size-Selected Au and Pd Clusters in Aberration-Corrected HAADF-STEM. *J. Phys.: Conf. Ser.* **2012**, *371*, 012010.